minerals

MDPI

Article

SO_2-Induced Aging of Hematite- and Cinnabar-Based Tempera Paint Mock-Ups: Influence of Binder Type/Pigment Size and Composition

José Santiago Pozo-Antonio [1], Daniel Jiménez-Desmond [1,*], Lara De Villalobos [1], Ana Mato [1], Amélia Dionísio [2], Teresa Rivas [1] and Carolina Cardell [3]

[1] CINTECX, GESSMin Group, Dpto. de Enxeñaría de Recursos Naturais e Medio Ambiente, Universidade de Vigo, 36310 Vigo, Spain
[2] CERENA, Instituto Superior Técnico, Universidade de Lisboa, 1049-001 Lisbon, Portugal
[3] Department of Mineralogy and Petrology, Faculty of Science, University of Granada, 18071 Granada, Spain
* Correspondence: danieljose.jimenez@uvigo.es

Abstract: Hematite- and cinnabar-based paint mock-ups prepared with either rabbit glue or egg yolk binder were artificially aged in an SO_2-rich atmosphere, as a model system for investigating the deterioration of tempera paints exposed to an industrial atmosphere. The overall research aim was to identify the type of degradation occurring in tempera paints and the different alteration mechanisms related to the physical, mineralogical and chemical characteristics of the paint. Tempera mock-ups were prepared by mixing binder (egg yolk or rabbit glue) and pigment (cinnabar of different particle sizes or hematite) and were then exposed to SO_2 for 2 months in accelerated aging tests. The colour, gloss, reflectance, roughness and micro-texture of the surfaces of the mock-ups were determined before and after the tests. In addition, chemical and mineralogical changes were determined by X-ray Powder Diffraction (XRPD), Attenuated Total Reflection-Fourier Transform Infrared spectroscopy (ATR-FTIR) and Scanning Electron Microscopy with Energy-Dispersive X-ray Spectroscopy (SEM-EDS) analysis. Colorimetric changes were confirmed, mainly in the cinnabar-based paints containing egg yolk, and in the hematite-based paints containing rabbit glue. Neoformed mineral phases have not been detected by XRPD, but precipitation of gypsum on the exposed surfaces has been confirmed by SEM. For cinnabar-based paints, the amount of sulfate-rich deposits was higher on egg yolk mock-ups than on rabbit glue samples, though the opposite was observed for the hematite-based paints. This confirmed the influence of the binder composition and pigment-binder tandem in the susceptibility to SO_2 deposition. Pigment particle size did not have a clear influence on the physical and chemical changes in the tempera mock-ups during the ageing tests.

Keywords: tempera mock-up; sulphation; egg yolk; rabbit glue; accelerated aging

Citation: Pozo-Antonio, J.S.; Jiménez-Desmond, D.; De Villalobos, L.; Mato, A.; Dionísio, A.; Rivas, T.; Cardell, C. SO_2-Induced Aging of Hematite- and Cinnabar-Based Tempera Paint Mock-Ups: Influence of Binder Type/Pigment Size and Composition. *Minerals* **2023**, *13*, 289. https://doi.org/10.3390/min13020289

Academic Editor: Alberto De Bonis

Received: 11 November 2022
Revised: 14 February 2023
Accepted: 16 February 2023
Published: 18 February 2023

1. Introduction

Historical paintings undergo different aging processes due to interactions between the paint and various agents such as solar radiation, rain and pollutant gases and particles [1–6]. The composition of medieval tempera paints (comprising a mixture of inorganic pigments and an organic egg yolk or rabbit glue binder) causes them to suffer physical modifications due to interactions with alteration agents such as the gaseous pollutants CO_2, NO_x, SO_2 and O_3, commonly found in industrial atmospheres. Accelerated aging tests can be used to determine the effect of these gases on the physical properties of paintings [7]. However, previous research studies have mainly involved ozone [8–12] and nitrogen oxides, specifically NO_2 mixed with SO_2 [13–20]. Thus, although SO_2 can have potentially damaging effects, previous studies have not considered the effects of SO_2 gas alone on tempera paints, probably because the atmospheric concentrations of this gas have declined in recent years as a result of the implementation of European Union policy measures [21]. Therefore, not

only can the materials of the oldest constructions show deterioration due to interaction with SO_2, but also, SO_2-induced damage to the building materials (e.g., stone) used in cultural heritage still occurs in cities exposed to volcanic emissions and in polluted metropolitan areas [22–24]. In paintings, the damage caused by pollutant gases seems to be greatly influenced by the type of pigment (composition and granulometry) and the type of binder contained in the paint. Thus, impurities in the pigments historically used in tempera paints greatly influence the chemical and physical properties of the pigments [5,25,26] and consequently their deterioration [27,28]. Other studies, focused on the deterioration of tempera paint mock-ups exposed to artificial UV light and outdoor atmospheres, have demonstrated the influence of pigment impurities and grain size in the deterioration processes [5,29–31]. Specifically, regarding the decay of tempera paints due to SO_2 deposition, Herrera et al. [31] confirmed that tempera paints made with pigments containing portlandite as an impurity underwent faster sulphation than tempera paints made with pigments containing only calcite.

In addition to the pigment composition and grain size, the interactions between the pigments and binders also influence the deterioration (as observed by the present authors in previous studies [27,28]) in which tempera paint mock-ups made with blue smalt, lapis lazuli and azurite, and green malachite pigments of different particle sizes, and with rabbit glue or egg yolk binder, were exposed to SO_2 gas. The current article is the third in a series involving the exposure of tempera paints to a SO_2-rich atmosphere, and it focuses on tempera paints made with two red pigments, hematite and cinnabar, with very different levels of susceptibility to chemical alteration. The aim of the study was to obtain further information about the influence on SO_2-induced damage of mineralogical aspects of the pigments (chemistry and crystal structure) and their grain size, also considering the influence of the interaction between the pigment and the binder. Information about the response of tempera paints mock-ups exposed to SO_2 will be useful for decision-making regarding the application of preventive conservation measures, and/or the selection of replacement materials for the conservation of tempera paintwork exposed to high atmospheric concentrations of SO_2.

Hematite and cinnabar are some of the most common pigments used to make red tempera paint. The mineral hematite (Fe_2O_3) began to be used as pigment in Paleolithic times [32]. It was used with ochre goethite, black manganese oxides and charcoal, which together made up the early prehistoric painter's palette. Darkening has been reported to be the most common type of deterioration pattern in this type of painting. The darkening is mainly caused by the incipient conversion of hematite (Fe_2O_3) to magnetite (Fe_3O_4) when hematite is exposed to humid air and a reducing agent, such as SO_2 [1,33]. Moreover, orange staining has also been observed at high relative humidity, i.e., higher than 80% [34,35]; this may be caused by water in the surroundings interacting with the hematite to create OH^- ligands, and thus reduce the symmetry around the Fe^{3+} ions. The red hue is less saturated when there is greater distortion around the Fe^{3+} ions [36].

Cinnabar is a mercury sulphide mineral (α-HgS) which has been used as a pigment since Neolithic times [37] and was greatly appreciated during the Middle Ages and in the Renaissance and Baroque periods [38]. Although cinnabar is generally considered resistant, darkening of paints containing this pigment is common. Different possible pathways for the darkening of cinnabar during light exposure have been considered: (i) formation of black metacinnabar (β-HgS) [39,40], (ii) formation of a thin layer of black colloidal mercury (Hg) [41], (iii) formation of metallic mercury (Hg) due to the intervention of chlorides, either as a catalyst in the redox reaction of cinnabar or as intermediate reaction products that are subsequently photochemically reduced [42–44], and (iv) in the absence of chlorides, reduction to metallic mercury (Hg) via photo-induced electron transfer when cinnabar pigments are exposed to UV-C at room temperature and high relative humidity [45]. Moreover, in the absence of light, transformation of α- to β-HgS can be induced by temperatures higher than 350 °C [46–50].

In addition to the pigment deterioration, the interactions between the binder and atmospheric agents should also be taken into account. In previous studies involving tempera paints exposed to an artificial SO_2-rich atmosphere, we found that egg tempera underwent yellowing and opacification, and that in tempera paint containing rabbit glue, loss of the binder led to the formation of new fissures [27,28]. However, the organic binder delayed the reaction between lime-based paints and atmospheric SO_2 [31].

Regarding preventive conservation strategies for tempera paints, we considered that the effect of SO_2 on hematite- and cinnabar-based tempera mock-ups should be evaluated because (i) sulphation occurs in lime-, lapis lazuli-, smalt-, azurite- and malachite-based paints containing either egg yolk or rabbit glue binder [27,28,31], with calcium, magnesium, potassium or sodium sulfate-rich salts previously found on the surface [27,28] of tempera mock-ups exposed to an SO_2-rich atmosphere, and (ii) the effect of SO_2 exposure on the deterioration of tempera paints containing hematite or cinnabar has not previous been studied. In the present study, we evaluated the effects of exposure to SO_2 gas on the physical and chemical properties of tempera paint mock-ups made with different red pigments (hematite or cinnabar) and binders (egg yolk or rabbit glue). In addition, cinnabar pigments of different particle sizes were used to investigate the influence of particle size on the degree of deterioration. The physical properties of the paints studied were the appearance, colour, gloss, reflectance, roughness and micro-texture. Chemical changes in mock-ups, as well as the neoformed minerals after exposure of the paint mock-ups to SO_2 were determined by X-ray Powder Diffraction (XRPD), Attenuated Total Reflection-Fourier Transform Infrared spectroscopy (ATR-FTIR) and Scanning Electron Microscopy with Energy-Dispersive X-Ray Spectroscopy (SEM-EDS). In addition, the raw materials (binders and pigments) were also characterized in detail by XRPD and SEM-EDS analysis.

2. Materials and Methods

2.1. Preparation of Mock-Ups

Ten tempera paint mock-ups were used in the study. The paints were prepared as binary mixtures of hematite (1 particle size), or cinnabar (4 different particle sizes) mixed with egg yolk or rabbit glue binder (the codes used to identify the components are shown in Table 1). All pigments were supplied by Kremer Pigments GmbH & Co. KG (Aichstetten, Germany), except for CIN-ST, which was provided by CAREMI S.L. (Seville, Spain). The egg yolk binder (albumin, ovalbumin and fatty acids) was made in the laboratory using locally purchased eggs, and rabbit glue pearls (collagen, ref. 63,028) were obtained from Kremer Pigments GmbH & Co. KG (Aichstetten, Germany).

Cinnabar pigments of different particle sizes were used. Information on the particle size of the pigments (Table 1) was obtained from the manufacturers (Kremer Pigments GmbH & Co. KG and CAREMI S.L) and from our previous studies [5,25] using laser diffraction particle size analysis. Some significant differences in particle size distribution relative to the values reported by the manufacturers were confirmed, specifically for the cinnabar standard (CIN-ST), for which the manufacturer indicates a particle size less than 120 μm, while laser diffraction analysis yielded a main maximum particle size of 8 μm and a range of 2–25 μm. Therefore, CIN-ST was the finest cinnabar pigment included in the study (Table 1).

Paint mock-ups were prepared according to Old Master recipes [51]. The procedures used to prepare the egg yolk-based paints and the rabbit glue-based paints are described in detail by Herrera et al. [3] and Cardell et al. [29], respectively. The paint mixtures (inorganic pigment and organic binder) were prepared in accordance with organoleptic parameters. The tempera paints thus prepared contained varying amounts of organic binder, depending on the chemical composition and particle size of the pigment: finer grained pigments usually require more binder [25]. Thus, 0.5 g of each pigment was mixed with the required amount of binder. For the egg yolk-based tempera paints [3], the egg yolk was carefully separated from the white and was then rolled onto a paper tissue to remove the layer of adhering egg white and most of the chalazae. The skin at the bottom of the yolk was

punctured with a pin, and the liquid content was poured into a jar. The powdered pigment (0.5 g) was placed in a small bowl and several drops of beaten egg yolk or prepared rabbit glue were added to form a fluid paste. Droplets of binder were added until the required consistency was reached, i.e., when droplets formed at the tip of the brush did not fall off easily.

Table 1. Properties of the pigments according to the manufacturers and to the authors of this study. *: Main maximum particle size and particle size range in brackets. Hematite: Fe_2O_3; Dolomite: $CaMg(CO_3)_2$; Quartz: SiO_2; Cinnabar: HgS.

Identification Code	Commercial Identification Code	Mineralogical Composition According to Manufacturer	Mineralogical Composition According to Authors	Grain size (μm) According to Manufacturer	Grain Size (μm) According to [5,25] *
HE	Hematite, 48,651	Hematite	Hematite Dolomite Quartz	1.5	0.6 (0.3–17)
CIN-EF	Cinnabar very fine, 10,624	Cinnabar	Cinnabar Quartz	<20	12 (0.4–40)
CIN-M	Cinnabar medium, 10,627	Cinnabar	Cinnabar Quartz	50–63	48 (15–90)
CIN-C	Cinnabar dark, 10,628	Cinnabar	Cinnabar Quartz	63–100	75 (10–130)
CIN-ST	Cinnabar standard, HGS PR 106	Cinnabar	Cinnabar Quartz	<120	8 (2–25)

The prepared mixtures were applied to glass microscope slides (ca. 75 mm × 25 mm × 1 mm) with a paintbrush. Several layers of paint were applied, each being applied after the previous layer was completely dry (at least 6 h between applications). The paint mock-ups were identified by a code, including the letter E for egg yolk or R for rabbit glue in addition to the letter denoting pigment, to clearly differentiate the powder pigments from the binary paint mixtures (Table 2). Binders without pigments were also applied directly to the microscope slides for determining the texture and composition of the binders. Once the microscope slides were adequately covered by the paint, they were held under laboratory-controlled conditions (18 ± 5 °C; 60 ± 10% RH) in darkness for 1 month.

Table 2. Mineralogical composition of the tempera mock-ups before and after the aging test, as determined by XRPD, and characteristics detected by FTIR and SEM-EDS after the aging test. See Table 1 for an explanation of the identification codes. The last letter of the identification code refers to type of binder: E represents egg yolk and R, rabbit glue. Hematite: Fe_2O_3; Quartz: SiO_2; Cinnabar: HgS.

Identification Code	XRPD before SO_2 Test	XRPD after SO_2 Test	New FTIR Bands after SO_2 Test	New SEM-EDS Features after SO_2 Test
HE-EF-E	Hematite	Hematite	-	Ca and S-rich fibrous particles (with some Fe, Na, Si, Mg, P, K and Ti). More abundant in R-samples than in E-samples.
HE-EF-R	Hematite	Hematite	-	
CIN-ST-E	Cinnabar	Cinnabar	1090 cm^{-1}: S–O str.	Ca and S-rich fibrous particles (with some Na, Al, Mg, Si, P, K and Fe). More abundant in E-samples than in R-samples. Ca and S-rich acicular crystals (with some Na, K and P). More abundant in E-samples than in R-samples.
CIN-ST-R	Cinnabar	Cinnabar	-	
CIN-EF-E	Cinnabar	Cinnabar	1090 cm^{-1}: S–O str.	
CIN-EF-R	Cinnabar	Cinnabar	1090 cm^{-1}: S–O str.	
CIN-M-E	Cinnabar	Cinnabar	1090 cm^{-1}: S–O str.	
CIN-M-R	Cinnabar	Cinnabar	-	
CIN-C-E	Cinnabar, Quartz	Cinnabar	1090 cm^{-1}: S–O str.	
CIN-C-R	Cinnabar, Quartz	Cinnabar	-	

Each slide was then cut in two pieces: one piece (ca. 25 mm × 25 mm × 1 mm) was used for reference purposes and the other piece (ca. 50 mm × 25 mm × 1 mm) was subjected to the accelerated aging test.

2.2. Artificial Aging Tests

The prepared samples were exposed to SO_2 in a FITOCLIMA 300EDTU climatic chamber (25 °C; 45% RH) for two months. The SO_2 was diluted (to 3%) in 3000 ppm of nitrogen and applied at a concentration of 200 ppm, which is more than 250,000 times higher than the current SO_2 concentrations in most European cities (average value 0.00076 ppm) [21].

In a previous study [27], the water used in the chamber was characterized by high performance liquid chromatography (HPLC) (Metrohm chromatograph with a Metrosep A Supp 5–250 column), to determine the concentrations of chloride, nitrite, nitrate and sulphate (Cl^-, $NO_2{}^-$, $NO_3{}^-$ and $SO_4{}^{2-}$ respectively). The water contained 15.8 mg/L Cl^-, <0.05 mg/L $NO_2{}^-$, 2.15 mg/L $NO_3{}^-$ and 23.7 mg/L $SO_4{}^{2-}$ [27]. Additional analysis of the water, by Inductively Coupled Plasma-Optical Emission Spectrometry (ICP-OES) (Perkin Elmer Optima 4300 DV ICP-EPS) showed that the water contained 0.017 mg/L Ba^{2+}, 17.35 mg/L Ca^{2+}, 2.37 mg/L K^+, 3.74 mg/L Mg^{2+} and 13.18 mg/L Na^{2+} [27].

2.3. Analytical Techniques

Powdered pigments were analysed by X-ray Powder Diffraction (XRPD) (Siemens D5000) (KS Analytical Systems, Aubrey, TX, USA) to determine the mineralogical composition. The analysis was performed using Cu-Kα radiation with a Ni filter, voltage of 45 kV and intensity of 40 mA. The exploration range was 3° to 60° 2θ and the goniometer speed was 0.05° 2θ s^{-1}. The minerals were identified using the X'Pert Highscore software.

The binders and the powdered pigments were also examined by Scanning Electron Microscopy (SEM) with Energy-Dispersive X-ray Spectroscopy (EDS) (FEI Quanta 200) (FEI Company, Hillsboro, OR, USA). Optimum observation conditions were obtained at an accelerating potential of 15–20 kV and a working distance of 9–11 mm. These samples were also examined in a high-resolution Schottky-type Field Emission Scanning Electron Microscope (FESEM) coupled to an energy dispersive X-ray spectrometer (EDS) (Zeiss Auriga SEM) (ZEISS, Jena, Germany). The instrument settings were 10^{-4} Pa vacuum and 3 kV beam accelerating voltage. Samples were mounted on Al stubs with double-sided adhesive C tape and were examined using both Secondary Electron (SE) and Backscattered Electron (BSE) detectors.

The physical features of the aged and reference samples were evaluated using the following protocol, as in previous studies [27,28]:

- The differences in appearance of the aged and reference samples were determined by stereoscopic examination (Nikon SMZ 1000) (Nikon Instruments Inc., Amstelveen, The Netherlands).
- The colour was characterized using CIELAB and CIELCH colour spaces [52,53], by spectrophotometric analysis (using a Minolta CM-700d) (Konica Minolta, Chiyoda, Tokyo, Japan). The parameters measured were L* (lightness) and the polar coordinates a* and b*. L* is the lightness ranging from 0 (absolute black) to 100 (absolute white); a* indicates the colour position between red (positive values) and green (negative values) and b* between yellow (positive values) and blue (negative values). Nine measurements were made at random on each sample to provide statistically consistent results. The measurements were made in the Specular Component Included (SCI) mode, for a spot diameter of 3 mm, with D65 as the illuminant and observer angle of 10°. Colour differences ΔL*, Δa* and Δb* and the total colour difference (ΔE^*_{ab}) between the reference and the aged samples were computed [52,53]. Note that higher values indicate more visible colour difference.
- Gloss measurements (3 per sample) were made with a gloss meter (Konica Minolta Unigloss 60Plus) (Konica Minolta, Chiyoda, Tokyo, Japan) with a reflection angle

of 60°. The difference in gloss (ΔG) between the aged and the reference paints was afterward calculated. Standard deviations were also calculated.

- The change in reflectance was determined using a hyperspectral camera, with a combination of an imaging spectrograph and a monochrome matrix array sensor. The equipment consisted of a CCD sensor (Pulnix TM-1327 GE) (PULNiX America Inc, Orleans, USA) (1040 rows, 1392 columns) with an objective lens of focal length 10 mm. A spectrograph (ImSpector V10) (Specim, Oulu, Finland) with a spectral range of 400–1000 nm and a spectral resolution of 4.55 nm was positioned between the sensor and the lens. The spectral camera recorded a linear array of 1392 pixels at 1040 wavelengths in the range 400–1000 nm. The target sample was moved vertically, and the camera scanned the surface line by line to obtain an image at each of the 1040 wavelengths. The light source was an incandescent lamp (Schott DCR® III) with a rectangular head (length 51 mm and width 0.89 mm). The light was focused by a cylindrical lens placed in front of the lamp, and the illuminated area was thus 15 cm long and 1 cm wide. The sample was placed on a motorized XYZ translation stage in which the Z- axis was perpendicular to the sample surface to allow displacement. The paint mock-ups were fully scanned. Once the hyperspectral images were acquired, the data were processed in a MATLAB programming environment to display the respective reflectance graphs.
- Roughness was characterized with a profilometer (Mitutoyo SJ400) (Gipuzkoa, Basque Country, Spain) to assess the morphological alterations of the aged surfaces from the arithmetic average roughness (Ra, μm), root mean square roughness (Rq, μm) and average maximum profile height (Rz, μm) described in [54]. The equipment traced a scan of 2 cm length. For each sample, 3 profiles were obtained and the average values of Ra, Rq and Rz (and the corresponding standard deviations) were calculated.

The mineralogical and chemical composition of the reference and aged tempera mock-ups were studied using the following techniques, to help understand the physical changes detected in the aged samples:

- Mineralogical composition was determined by XRPD analysis, as previously reported. Small scales (c.a. 0.8 cm^2) were extracted from the mock-ups with a scalpel and were ground and homogenized before analysis (Siemens D5000).
- The molecular composition was determined by means of Attenuated Transmittance Reflectance Fourier–Transform Infrared Spectroscopy (ATR-FTIR) (Thermo Nicolet 6700) (ThermoFisher Scientific, Waltham, MA, USA). Infrared spectra were recorded at a 2 cm^{-1} resolution over 100 scans from 400 to 4000 cm^{-1}. The powdered samples analysed by XRPD were used in this analytical technique.
- Micro-texture and composition were studied by Scanning Electron Microscopy (SEM) with Energy-Dispersive X-Ray Spectroscopy (EDS) (Philips XL30) (FEI Company, Hillsboro, OR, USA), with both Secondary Electron (SE) and Backscattered Electron (BSE) detectors. Optimum observation conditions were obtained at an accelerating potential of 15–20 kV and a working distance of 9–11 mm.

To determine the presence of salts in the tempera paints, the hydrophobic behaviour of the reference samples was characterized by the static contact angle, measured by method BS EN828:2013 [55] (the sessile drop method), with a goniometer (SEO Phoenix-300 Touch) (Kromtech, Bangalore, India). A droplet of 6 μL of deionized water was placed on the sample surface. The measurements were made at room temperature (18 ± 5 °C), and a total of three measurements per sample were considered. The strong interaction between the paints and the water used in the aging test can be explained by small static contact angles, as the water drops would wet the surface of the paint.

3. Results and Discussion

3.1. Powdered Pigments and Reference Mock-ups

Analysis of the mineralogical composition revealed that both types of pigment contained quartz (SiO_2) as an impurity, and also that the hematite contained dolomite ($CaMg(CO_3)_2$) (Table 1). Detection of these impurities suggests that the pigments are of natural origin, as the compounds identified are not of the types intentionally added to improve specific characteristics of the paints [26]. The mineralogical composition of the tempera paint mock-ups was generally consistent with that of the corresponding pigments. However, the impurities (dolomite and quartz) were not detected in all paint samples (Table 2), probably because they were sometime present at concentrations below the detection limit of the XRPD technique (2%–3% in weight).

SEM analysis of the binder samples revealed the different texture and composition of both binders (Figure 1A,B). The egg yolk binder had pores (of diameter of up to 20 µm) in a C-rich layer with some P, S and Cl (Figure 1A). C-rich deposits containing Na, Mg, Si, P, Cl and Ca were also detected in this layer. The rabbit glue had a more regular texture (a continuous C-rich layer with few pores of smaller diameter) and contained some Na, S, Cl and Ca.

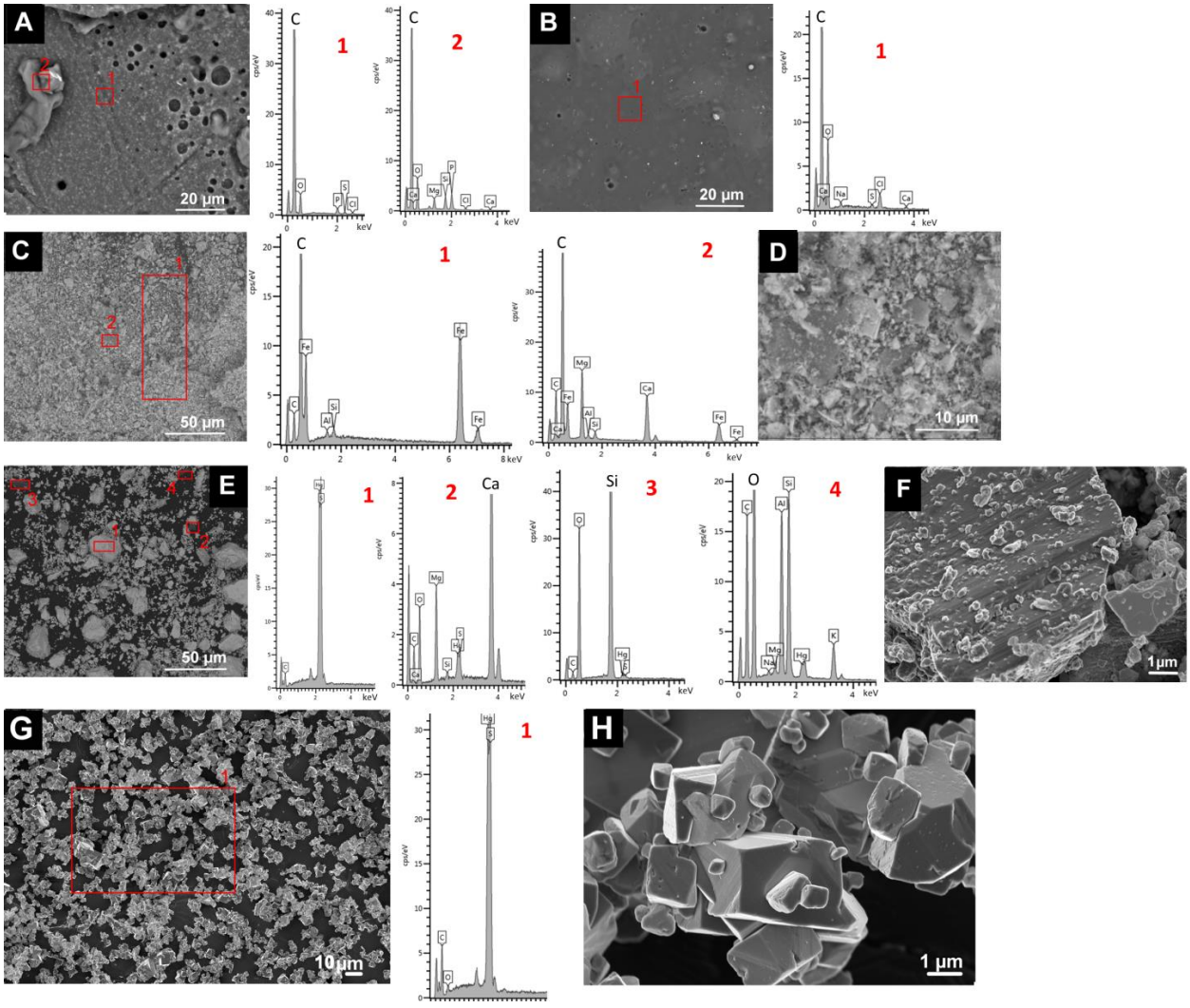

Figure 1. SEM micrographs and EDS spectra of the binders and the pigments used in this study. (**A**): egg yolk binder. (**B**): rabbit glue binder. (**C**,**D**): HE; (**E**,**F**): CIN-EF and (**G**,**H**): CIN-ST. See Table 1 for explanation of the identification codes.

SEM analysis of the pigment samples confirmed the mineralogical composition determined by XRPD and revealed the presence of other mineral phases not detected by XRPD. The hematite was composed of a mixture of acicular grains (of up to 5 μm) rich in Fe (corresponding to hematite grains) and also some grains rich in Si (corresponding to quartz as an impurity), some larger crystals (up to 30 μm) rich in Mg and Ca (Figure 1C,D), corresponding to the dolomite identified by XRPD, and also some grains rich in Si and Al (Figure 1C,D). Regarding the CIN pigments (Figure 1E–H), CIN-ST contained particles with a rhombohedral habit (Figure 1H), as previously observed [25]. This habit is characteristic of cinnabar pigment grains obtained by wet process [38]. In CIN-ST, only Hg and S, corresponding to cinnabar, were detected by EDS (Figure 1G). In the other CIN pigments (Figure 1E,F), particles with a different composition from that of cinnabar were detected: (i) particles rich in Mg and Ca; (ii) grains rich in Si (probably quartz detected by XRPD) and iii) particles rich in Al and Si with lower contents of K, Mg and Na.

Regarding the stereomicroscopic study of the paint mock-ups, the results revealed different textures and surface finishes for all the reference paints (shown on the right of each micrograph in Figure 1). The surfaces of the paints containing the finer pigments (HE, CIN-ST, and CIN-EF) were smoother than those of the paints made with the coarser pigments (CIN-M and CIN-C). The colour of the reference mock-ups containing the coarser pigments was also not as homogenous as in the reference paints made with finer pigments. In fact, in paints containing coarser particles, white particles identified by XRPD as quartz grains were found mixed with red particles corresponding to the red pigment. In all reference mock-ups, circular pockmarks attributed to relics of air bubbles were observed, regardless of the pigment grain size and binder used (Figure 2).

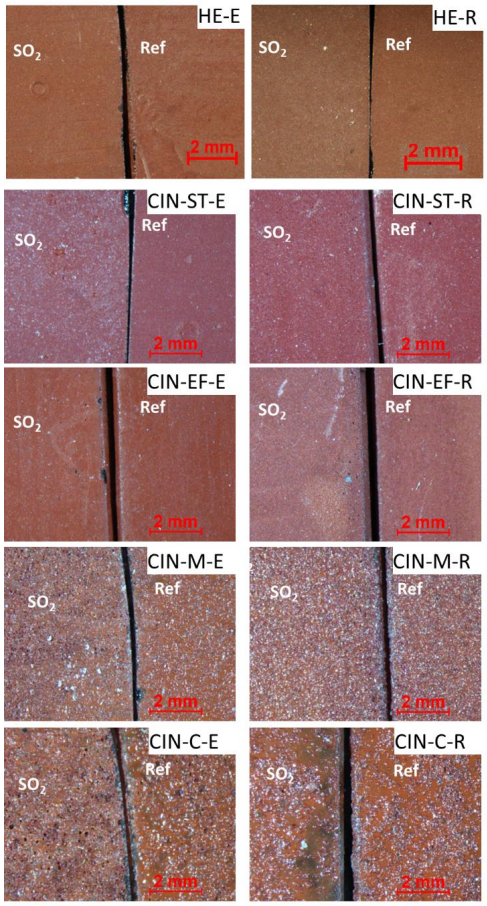

Figure 2. Micrographs of the red paint mock-ups: reference paints (Ref; on the **right** of each micrograph) and artificially aged paints (SO_2; on the **left**). See Table 1 for explanation of the identification codes.

3.2. Aged Tempera Mock-ups

The artificially aged paints containing the finer pigments (i.e., HE, CIN-ST and CIN-EF) did not show any changes in the visual appearance, except for CIN-ST-E and CIN-EF-R. In CIN-ST-E, white particles were observed on the surface, and in CIN-EF-R a yellowish area was observed (Figure 2). Regarding the coarser grained paints, white particles were observed in the CIN-M-E mock-up, while the CIN-M-R mock-up was not different from the respective reference sample (Figure 1). In the CIN-C-based paint sample containing egg yolk (CIN-C-E), voids formed after the aging test and darkening was observed in small, isolated areas of the mock-ups containing rabbit glue (CIN-C-R) (Figure 2).

Regarding the changes in colour (Figure 3), the total colour difference was highest for the CIN-C-E paint (ΔE^*_{ab} = 5.37 CIELAB units) and lowest for the HE-E paint (ΔE^*_{ab} = 0.94 CIELAB units). In the CIN paints, the colour difference was lowest in the CIN-M paints, regardless of the binder (ΔE^*_{ab} = 1.71 CIELAB units for the egg yolk-based paint and ΔE^*_{ab} = 1.88 CIELAB units for the paint containing rabbit glue). Therefore, the intensity of the colour change was not influenced by the particle size of the pigment.

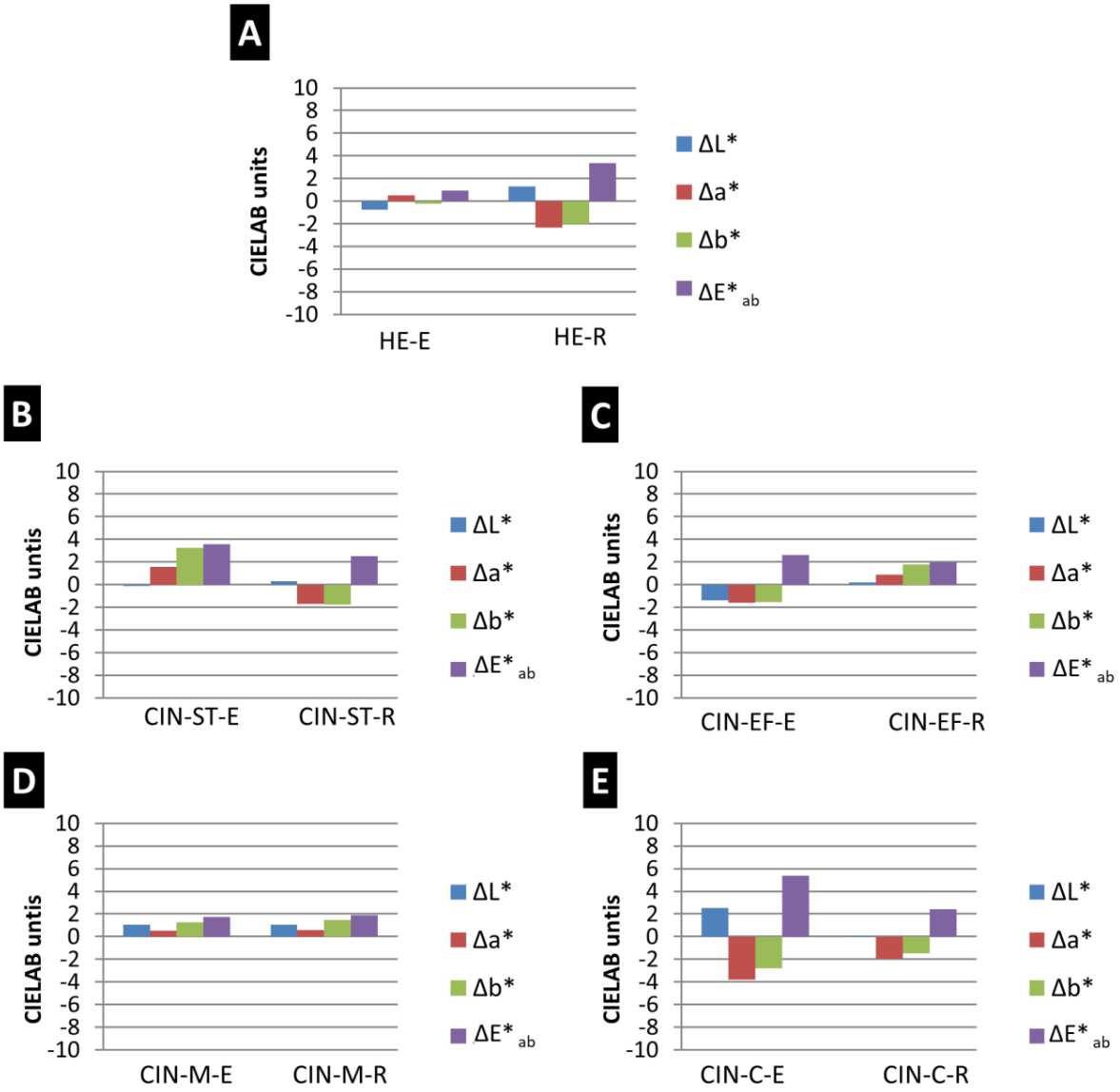

Figure 3. Differences in colour parameters (ΔL*, Δa* and Δb*) and total colour difference (ΔE^*_{ab}) in paint mock-ups exposed to SO_2 for two months. See Table 1 for explanation of the identification codes.

The colour parameters that varied most in the aging test were parameters a* and b*: a* mainly varied (decreased) in samples HE-R, CIN-EF-E and CIN-C (with both binders), and b* mainly varied in samples CIN-ST (with both binders; for the sample containing egg yolk, b* increased and for the sample containing rabbit glue, b* decreased), CIN-EF-R (b* increased) and CIN-M (samples containing each binder, b* increased). A decrease in a* indicates loss of reddish colour, and an increase in b* indicates an increase in yellowish tones. The L* parameter only varied notably in the HE-E mock-up (a decrease in L* indicates darkening of the surface).

The paint mock-ups in which changes were visible to an experienced observer without the aid of any instruments, i.e., $\Delta E^*_{ab} > 2$ CIELAB units [56], were HE-R, CIN-ST (for both binders), CIN-EF-E and CIN-C (for both binders). In addition, the ΔE^*_{ab} was higher in CIN-based paints containing egg yolk than in those containing rabbit glue (Figure 3). However, the opposite trend was observed for the HE-based paints.

The specular gloss of the paint mock-ups underwent slight changes, with the CIN-ST-E mock-up being the most strongly affected (ΔG of 3.53 $\pm$ 0.23 units, Figure 4). The gloss difference (ΔG) was lowest in the HE-based paints; in fact, the gloss did not vary in HE-E. Note that the changes in gloss were not related to the type of binder or particle size of the pigments.

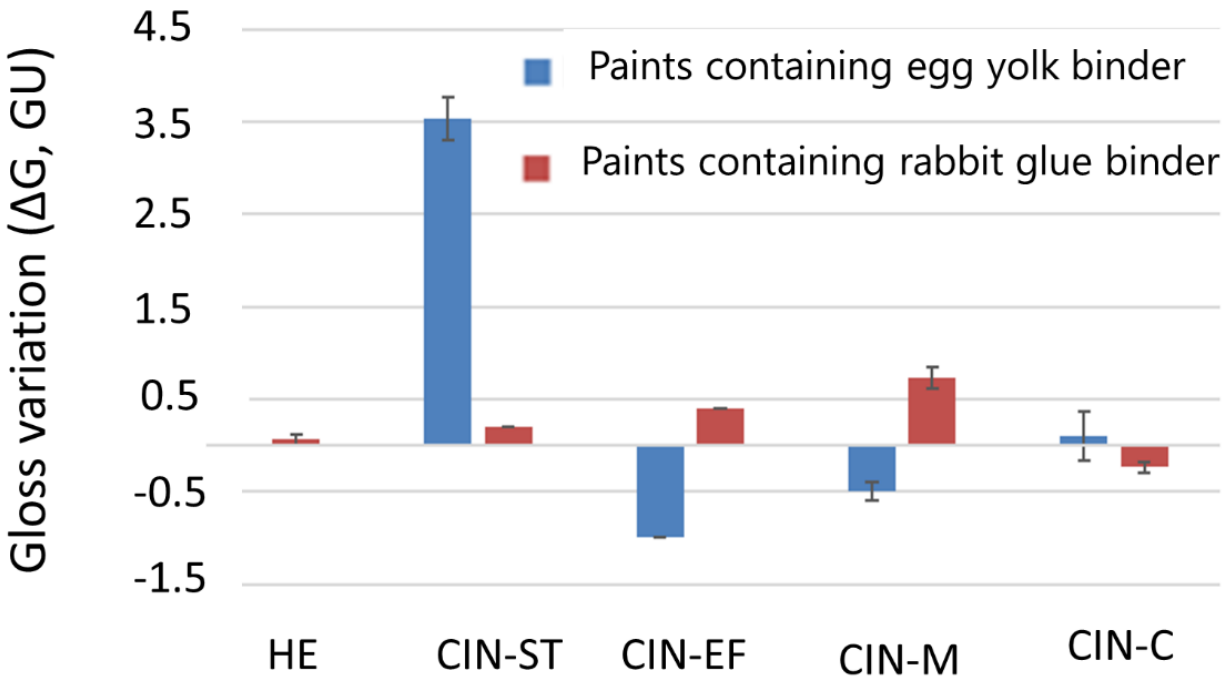

Figure 4. Gloss differences in the paint mock-ups after SO_2 exposure for two months. See Table 1 for explanation of the identification codes.

Although in most cases the paint reflectance did not undergo remarkable changes after SO_2 exposure, it was slightly higher in the aged paints than in the reference paints (Figure 5), except in the CIN-EF-E and CIN-M-E paint mock-ups. Regarding the spectral characteristics, slight displacement (40–50 nm) of a small reflectance band at around 510–500 nm toward lower wavelengths was detected in all mock-ups, except for CIN-C-R.

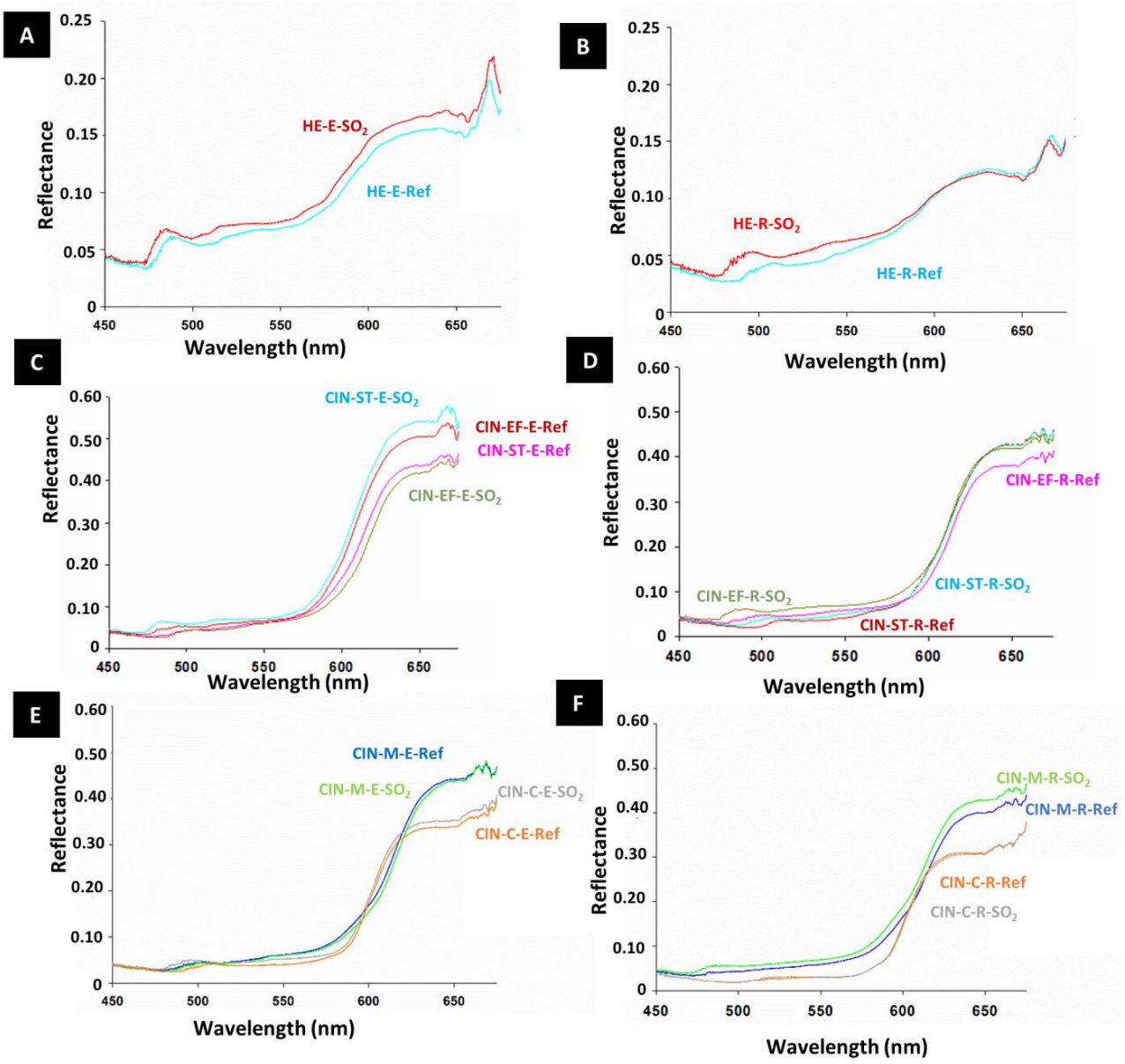

Figure 5. Reflectance spectra of reference paints (-Ref) and aged paints exposed to SO_2 (-SO_2) for two months. See Table 1 for explanation of the identification codes.

The values of the roughness parameters Ra (the arithmetic average roughness, μm), Rq (the root mean square roughness, μm) and Rz (the average maximum profile height, μm) before and after the aging test are shown in Figure 6. Interestingly, Rz underwent the greatest variation during the SO_2 test (Figure 6). An increase in Rz was detected after the aging test in the HE-E, CIN-ST-R, CIN-EF-E, CIN-EF-R, CIN-M-E, CIN-M-R and CIN-C-E mock-ups, while a decrease in Rz was observed in HE-R, CIN-ST-E and CIN-C-R mock-ups. However, owing to the wide range in the standard deviations, only the difference in the Rz value for the CIN-M-E paint before and after the test was statistically significant.

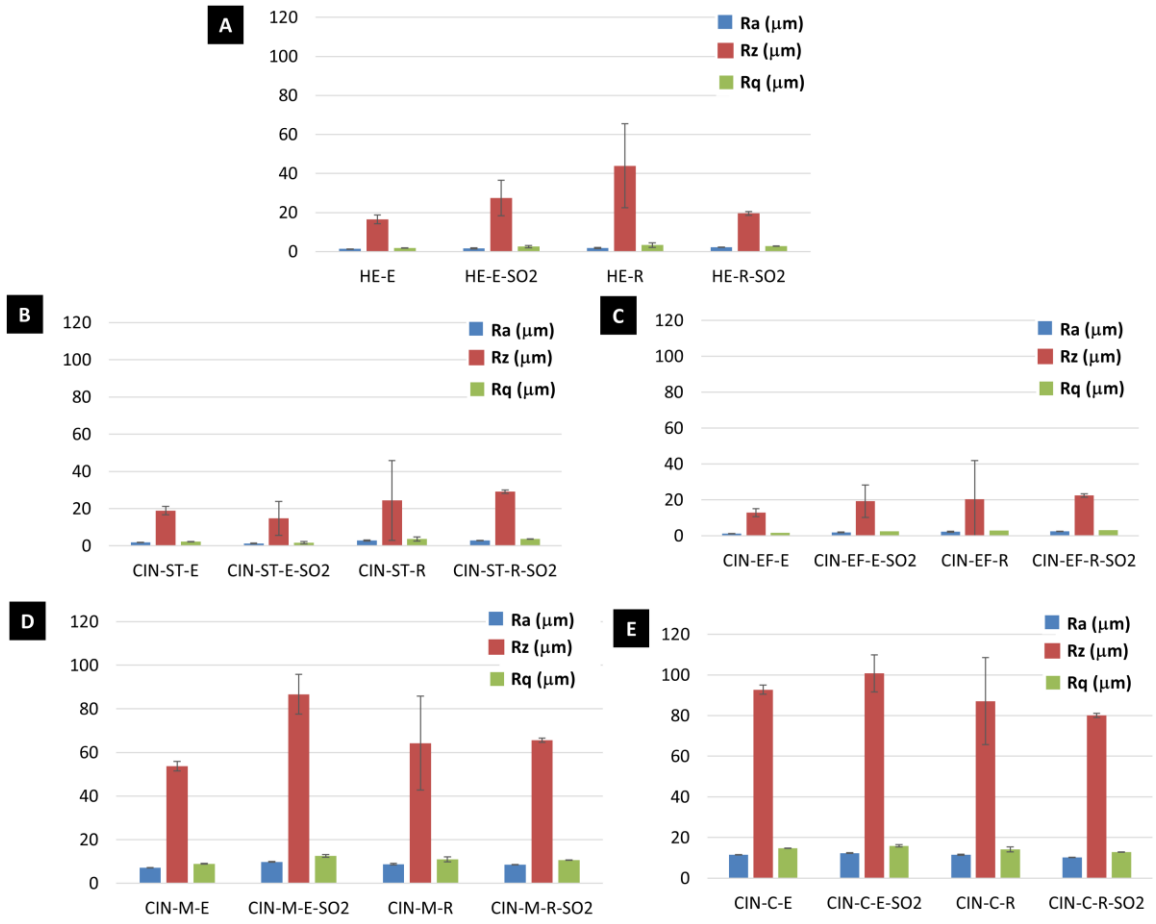

Figure 6. Roughness parameters (Ra, Rz and Rq) of the reference paints and the paints exposed to SO_2 (-SO_2) for two months. See Table 1 for an explanation of the identification codes.

By means of XRPD (Table 2), no neoformed mineral phases were detected in the hematite paints mock-ups exposed to SO_2 test. In the aged cinnabar temperas, new diffraction peaks were detected in both egg yolk- and rabbit glue-based samples, which have not been assigned to any phase given the uncertainty of their coincidence with the XRD main peaks of the most feasible mineral phases that have been considered, mainly sulphates (see Supplementary Materials).

The FTIR spectra of the reference and aged paints mock-ups are shown in Figure 7. Egg yolk binder (Figure 7A,C) was identified in the binder samples and in the reference samples by the absorbance bands at 3260 cm^{-1} (N-H stretching), 2973 cm^{-1} (cis double-bond stretching vibration of olefinic groups of unsaturated fatty acids), 2921 cm^{-1} ($\upsilon_{AS}(CH_2)$ stretching from long chain fatty acids), 2850 cm^{-1} ($\upsilon_{S}(CH_2)$ stretching in long chain fatty acids), 1730 cm^{-1} (ester C=O stretching band), 1625 cm^{-1} (C=O stretching in amide I), 1521 cm^{-1} (N–H in plane bending and of the C–N stretching in amide II), 1440 cm^{-1} and 1365 cm^{-1} (bending vibrations of CH_2 groups and CH_3 groups of amino acid side chain respectively), 1216 cm^{-1} (C-N stretching and N-H bending vibrations in amide III), 1135 cm^{-1} and 1041 cm^{-1} (stretching vibration of the C-O group of glycerol) and 956 cm^{-1} (twisting vibration of CH_2 group of glycerol) [57–59]. On the other hand, rabbit glue binder (Figure 7B,D) was detected in the binder and tempera paint reference samples from a wide band between 3300 cm^{-1} and 3100 cm^{-1} (N-H stretching), 2921 cm^{-1} ($\upsilon_{AS}(CH_2)$ stretching in long chain fatty acids), 1625 cm^{-1} (C=O stretching in amide I), 1521 cm^{-1} (N–H in plane bending and of the C–N stretching in amide II), and bands between 1450 and 1000 cm^{-1} associated with collagen absorption features attributed to CH_2 wagging, CH_3 deformation, C–N stretching and C–OH stretching) [29,60,61].

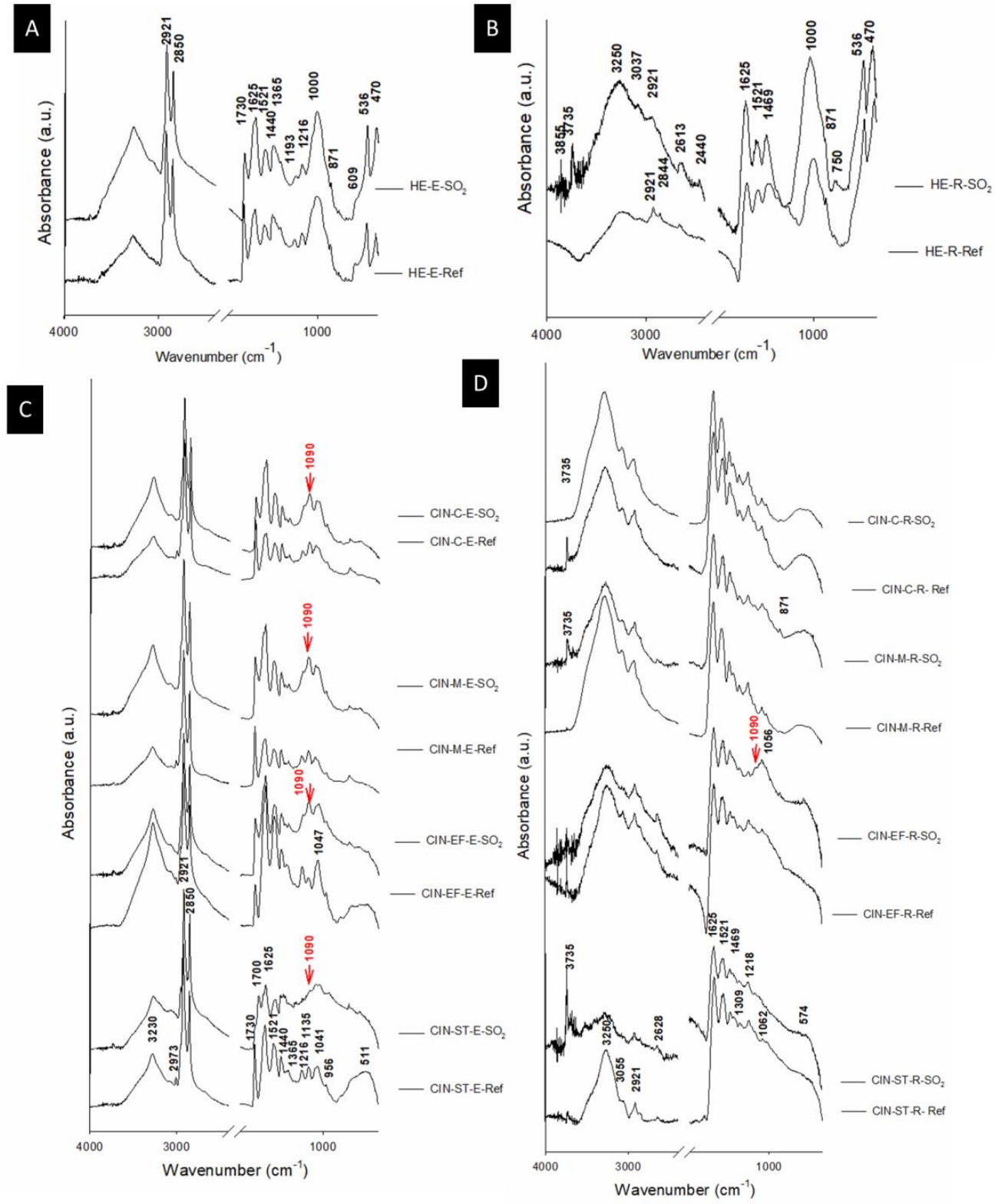

Figure 7. ATR-FTIR (absorbance) spectra of the reference paints (Ref) and the paints exposed to SO_2 (SO_2) for two months. See Table 1 for an explanation of the identification codes.

Hematite was identified in the FTIR spectra of the HE-based mock-ups, by bands at 536 and 470 cm^{-1} (Figure 7A,B) assigned to Fe-O [62]. Moreover, bands at around 1000 cm^{-1} were assigned to Si-O, which could be due to the presence of quartz as an impurity, although not identified by XRPD, probably because the mineral was present at an amount below the limit of detection of the method (2–3 wt%). However, in the powdered pigment, quartz was found in addition to dolomite. As a carbonate, dolomite was identified by strong absorption bands between 3050 and 2850 cm^{-1}, 2650 and 2500 cm^{-1}; 1790 and 1820 cm^{-1}; 1400 and 1500 cm^{-1}, and at 877 cm^{-1}, 730 cm^{-1} and 710 cm^{-1} [63], which were absent in the FTIR spectra of these paints (Figure 7A,B). Sulphated phases were not detected by XRPD or FTIR in the HE-based paints, regardless of the binder.

Regarding the CIN-based mock-ups, it is known that cinnabar does not absorb infrared radiation in the range of 4000–400 cm^{-1} [64]. In the aged CIN-based paints, a FTIR band at 1090 cm^{-1} (indicated by an arrow in Figure 7C,D and detailed in Table 2) is detected, which is assigned to S–O stretching [65] specifically in all paints containing egg yolk, as well as in the paint containing rabbit glue and CIN-EF. This finding would indicate that new sulphate phases were formed after the test, supporting the probable assignment as sulphates of the unassigned peaks found in XRPD spectra of CIN-based paints. However, the absence of S-O stretching band in the FTIR spectra of some of the rabbit glue-based mock-ups seems to indicate that sulphated salts concentration in their egg yolk counterparts was higher than those in the rabbit glue mock-ups.

Moreover, in the FTIR spectra of the artificially aged mock-ups containing egg yolk, a reduction in the intensity of the weak band at 2973 cm^{-1} was detected. In addition to ester linkages, double bonds are known primary sites of reaction in triglycerides, and their disappearance is indicative of a very advanced stage of oxidation [45,57]. The band at 1730 cm^{-1}, associated with ester carbonyl functional groups of triglycerides and phospholipids, also decreased gradually in intensity due to a reduction in ester linkages [45]. For the CIN-ST-E paint, the presence of a new band at 1700 cm^{-1} indicates the presence of free fatty acids due to the absorption by carbonyl double bonds (C=O stretching) [45]. Regarding the mock-ups containing rabbit glue, only the FTIR spectrum of paint CIN-ST-R showed a change, i.e., a decrease, in the intensity of the amide I at 1625 cm^{-1}, which suggests the presence of aggregated protein due to oxidation [66].

The comparative SEM-EDS study of the HE-based paints (Figure 8) before and after exposure to SO_2 showed the following: (1) before the test, the EDS analysis of the surface showed as majority chemical elements (wt%, average values): C (39.7 wt%), O (29.6 wt%), Fe (16.7 wt%), N (8.56 wt%) and lower amounts of Si (1.1 wt%), Al (0.7 wt%), S (0.5 wt%), Na (0.47 wt%), Mg (0.22 wt%) and P (0.01 wt%). It should be noted that in the reference samples made with rabbit glue neither P nor S is detected, which would be in line with the FTIR spectra; (2) after the test, deposits rich in S (15.2 wt%) and Ca (16.4 wt%) (atomic ratio 1:1) were identified; in the EDS spectra of these deposits, minor amounts of Na (1.55 wt%), Al (0.31 wt%) and Si (0.26 wt%) were detected. The fibrous habit of these deposits, together with their chemical composition, suggests that they correspond to gypsum. The S and Ca-rich deposits were much more abundant on the mock-up with rabbit glue (Figure 8D) rather than on the egg yolk-based mock-up (Figure 8C).

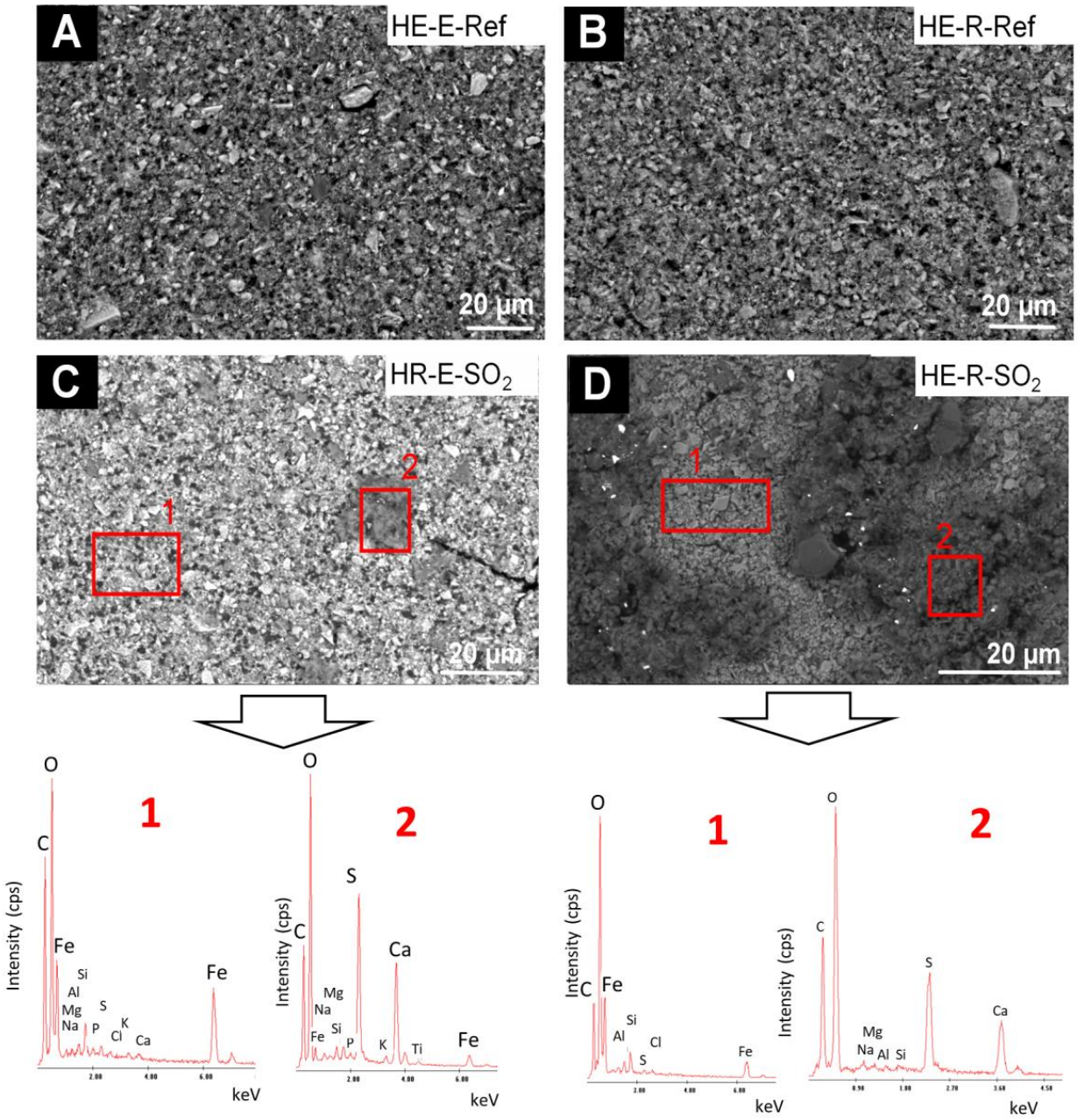

Figure 8. SEM micrographs and EDS spectra of the HE-based mock-ups. Ref indicates the reference paints and SO_2, the aged paints. See Table 2 for an explanation of the identification codes.

In the reference CIN-based mock-ups (Figures 9 and 10), SEM-EDS analyses showed as major elements (wt%, average values): C (30 wt%), O (8 wt%), Hg (52 wt%) and S (9 wt%) (Hg:S atomic ratio of 1:1). SEM examination of the reference paints and the aged revealed the presence of the following deposits on the SO_2 exposed mock-ups:

i. fibrous particles on CIN-ST-E-SO_2, CIN-EF-E-SO_2 and CIN-EF-R-SO_2 (Figure 9) and CIN-M-R-SO_2, CIN-M-E-SO_2 and CIN-C-R-SO_2 (Figure 10). A multi-particle analysis of these fibrous crystals resulted in an average of S and Ca weight content of 6% and 2%, respectively (S:Ca atomic ratio 2:1). Both their habit and their composition indicate with all certainty that they are gypsum crystals. The higher ratio of S to Ca may be due to the signal contribution of the cinnabar paint surrounding the crystals, which contains 9 wt% of S. These fibrous crystals were more abundant on the CIN-based paints containing egg yolk rather than on those containing rabbit glue. In some cases

(Figure 9F, EDS1), other deposits rich in S (3.4 atomic %) and Ca (12.3 atomic %), as well as in K (2.6 atomic %), have also been detected, which would suggest the possibility of the precipitation of sulphated salts rather than gypsum. In all these new deposits, other minor elements were detected in very low atomic percentages, such as Na (1.25%), K (2.73%), Mg (0.13%), Si (0.02%) and occasionally Cl (0.08%).

ii. crystals of acicular habit which were embedded in amorphous deposits such as those reported in i), or adhered to the organic phase (i.e., binder) of the paints (CIN-C-E-SO_2, Figure 10). These deposits were more abundant in the paints containing egg yolk and have a similar composition to the acicular deposits.

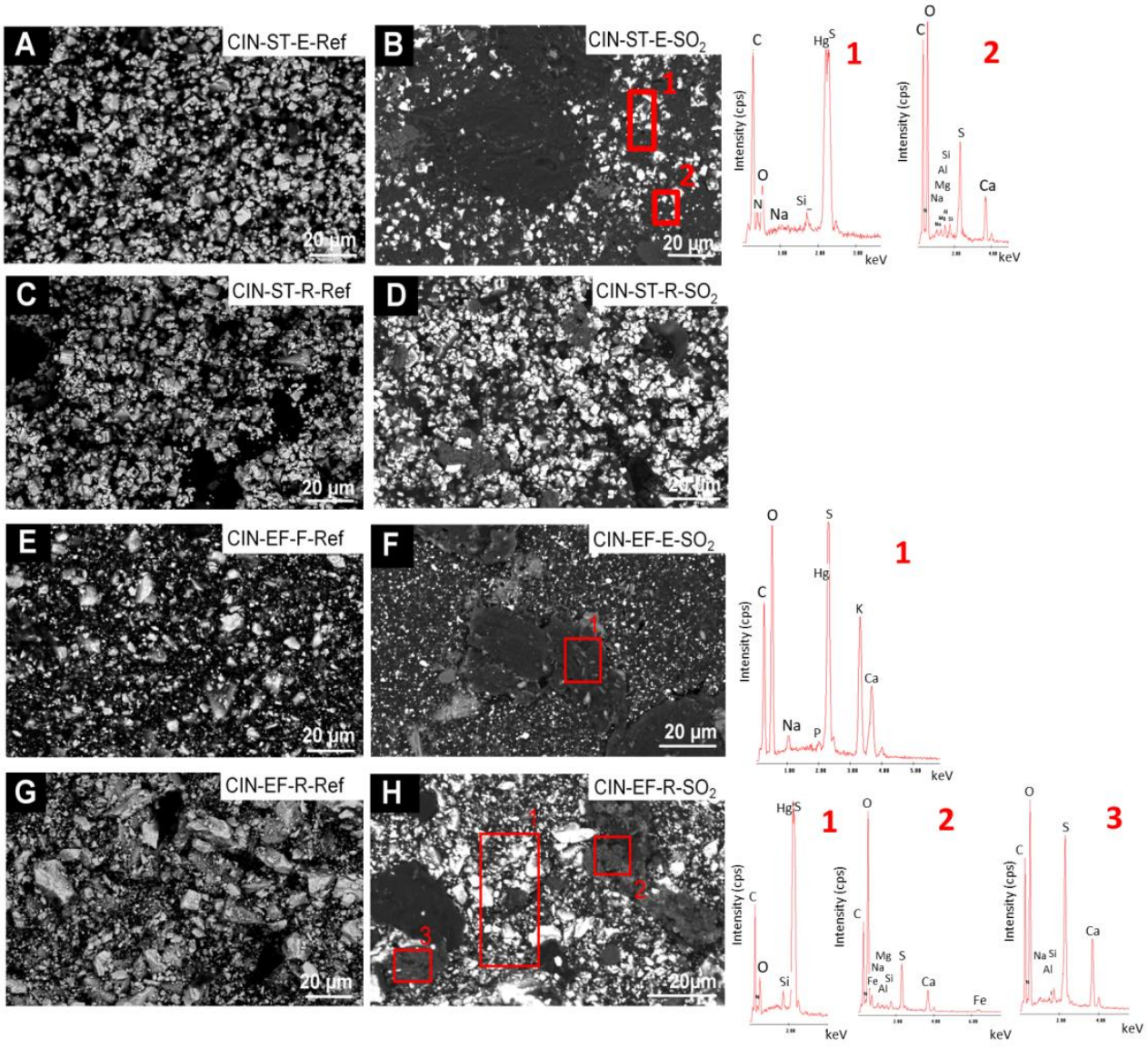

Figure 9. SEM micrographs and EDS spectra of the CIN-based mock-ups. Ref indicates the reference paints and SO_2 the aged paints. See Table 2 for an explanation of the identification codes.

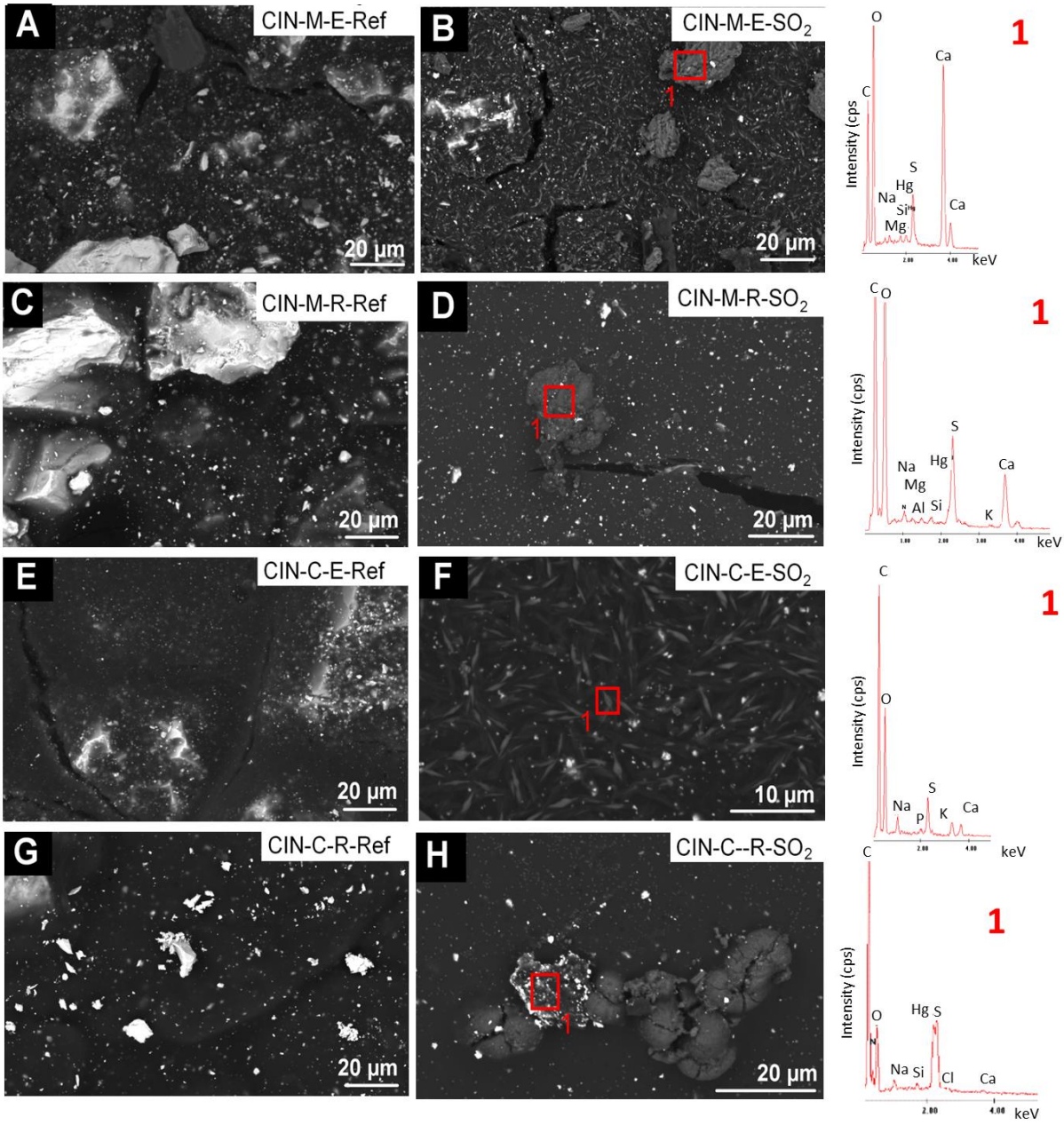

Figure 10. SEM micrographs and EDS spectra of the CIN-based mock-ups. Ref indicates the reference paints and SO_2 the aged paints. See Table 2 for an explanation of the identification codes.

Moreover, SEM enabled identification of fissures that formed during the aging test, regardless of the binder used (Figure 10B,D).

The static contact angle (Table 3) was higher in the mock-ups containing rabbit glue than in those containing egg yolk. Indeed, the static contact angle was higher than 90° in all the paints containing rabbit glue, except for CIN-C-R, indicating the hydrophobic nature of these paints [67]. Conversely, the static contact angle of the egg yolk CIN-based paints was less than 90°. Moreover, the static contact angle of the paints was inversely related to the pigment particle size, that is, coarser pigments yielded a smaller static contact angle in the corresponding paint.

Table 3. Static contact angle of the reference paint mock-ups. See Table 2 for an explanation of the identification codes.

Reference Paints	Static Contact Angle	STD
HE-E	89.45	3.88
HE-R	115.92	3.28
CIN-ST-E	89.03	5.71
CIN-ST-R	120.30	4.36
CIN-EF-E	78.10	1.18
CIN-EF-R	110.36	4.71
CIN-M-E	78.72	0.57
CIN-M-R	90.41	1.28
CIN-C-E	72.53	2.23
CIN-C-R	87.56	0.20

The nature of salts formed during the SO_2 aging test were identified by SEM-EDS, XRPD and FTIR analysis. SEM-EDS analysis revealed particles rich in S and Ca in paints containing both pigments (HE and CIN); the habits of these particles, similar to the characteristic acicular fibrous habit of $CaSO_2.2H_2O$ [68], indicate that these particles are gypsum. However, these phases were not detected by XRPD; possibly because of the type of sampling used in each technique: (1) in the SEM analysis, the surface of the sample was examined at very high magnification allowing identification of small deposits scattered on the surface; (2) in the XRPD analysis, the powder obtained by scratching of the paint layer was analysed. In this case, dilution of the newly formed crystals on the surface is expected, especially when these particles are present in small amounts on the surface (as was the case here); the dilution caused a relative decrease in concentration below the XRPD detection limit. FTIR analysis confirmed the presence of S-rich salt deposits in the CIN-paints by identification of bands assigned to the S–O stretching, consistent with the sulphate phases identified by SEM.

The following are possible sources of the ions forming these salts:

- Sulphur (S) probably originates mainly from the SO_2 gas; in the CIN-based mock-ups, the possible contribution from the chemical degradation of cinnabar cannot be ruled out, although there were no clear signs of damage in the cinnabar particles. Future research should focus on this possibility [45,69]. Sulphur was also detected at low concentration in the EDS spectra of the binder mock-ups, so another possible source, although in much smaller quantity, may come from the binder itself.
- Calcium (Ca) may originate from both binders and from the pigments, since in both hematite and cinnabars pigments, minor amounts of alkaline and alkaline earth elements were detected by SEM. In hematite mock-ups, Ca could also be derived from dolomite ($CaMg(CO_3)_2$), which was identified as an impurity in this pigment. Even though the water vapor that acts as a vehicle for the SO_2 gas in the chamber is produced by condensation after boiling, it cannot be ruled out a contamination from the water used in this process, which, as indicated in the previous section, it is not distilled water and contains a certain amount of alkaline and alkaline earth elements. This possibility was already considered in previous works [27,28].
- Potassium (K) is also present in minor amounts in the raw cinnabar pigments as K-rich impurities, and it may also come from the water used in the test (2.37 mg/L K^+ [27,28].
- Magnesium (Mg) was also identified as an impurity in both pigments (in hematite present as dolomite ($CaMg(CO_3)_2$) and also it may come from the binders, specially egg yolk binder. A contamination from water used in the chamber (3.74 mg/L Mg^{2+}) should not be ruled out [27,28].

SEM-EDS analysis enabled identification in the aforementioned deposits of Si, Na, K, Mg, Ti, P and Al in the HE-based mock-ups, and Si, Al, Na, P and Fe in the CIN-based mock-ups. Note that, as previously mentioned, Na, K, Mg and Cl were detected in the water used in the aging test (13.18 mg/L Na^{2+}, 2.37 mg/L K^{+}, 3.74 mg/L Mg^{2+} and 15.8 mg/L Cl^{-}, [27,28]). However, we attributed these elements to a background signal from the paint, either due to the binders or to impurities in the pigments. Thus, SEM-EDS analysis detected Si in the egg yolk binder, Na in both binders, Mg in the egg yolk, Cl in both binders and P in egg yolk. K was also assigned to egg yolk, as previously reported [3,45]. The Si signal could be related to quartz impurities in all the pigments, and Mg could also be derived from dolomite ($CaMg(CO_3)_2$) impurities. Regarding the Ti and Al detected in the HE-based paints, both may be formed by mineral phases, which although not detected by XRPD, may be present in the pigments according to the relevant literature. Thus, the presence of Ti may be related to the presence of TiO_2, as impurity usually found in natural hematite [70] and Al may be derived from impurities of type Al_2O_3, a mineral phase frequently found together with natural hematite bodies [70]. The same may apply to the Fe detected in CIN-based paint mock-ups, which may be derived from pyrite/marcasite (Fe_2S) impurities associated with natural cinnabar pigments [38,45].

SEM analysis revealed that, after the test, cinnabar mock-ups (regardless of the pigment particle size) made with egg yolk presented salt deposits in a greater quantity than in their counterparts made with rabbit glue. The opposite occurred regarding hematite paints: salt deposits were found to be more numerous in rabbit glue-based mock-ups. The lower static contact angles of the surfaces of cinnabar reference paintings made with egg, compared to those made with rabbit glue, probably favour a more intense interaction between the cinnabar egg-based paints and the water used in the aging test, as drops of water wet the surface and may penetrate the paint layer. Consequently, precipitation of a greater number of salts is more likely in this situation. In addition, the dissolved SO_2 in the water and/or the sulphates generated during aging of the paint should have penetrated the paints more easily. Therefore, it is more likely that the components of the tempera paints would be affected by exposure to SO_2 in the interior of the egg yolk-based paints than in the rabbit glue-based paints. However, this argument would not be applicable to the tempera made with hematite, in which the amount of saline deposits is greater in rabbit glue-based samples (which exhibit a higher static contact angle) than in those made with egg yolk (with a lower angle of contact). In this sense, there must be another variable involved in relation to the interaction between pigment and binder which explains the differences in the opposite behaviour between egg and rabbit within each type of tempera.

Salt deposition can be considered one of the causes of the colour change in the paints; in fact, in the CIN paints the colour change was greater in those containing egg yolk (deposition of more salts), and in the HE paints, it was greater in the samples containing rabbit glue (deposition of more salts). The fissures observed by SEM in the samples subjected to the accelerated aging test were undoubtedly due to the test itself since, in that case, fissures were also observed in the tempera mock-ups before being subjected to SO_2 exposition. It seems more likely that these fissures have formed as a consequence of the crystallization of the salts observed under SEM, although this fact must be confirmed by examination of cross sections. As the aging test was conducted under stable conditions of moisture and temperature, it is unlikely that the fissures were caused by retraction due to wetting-drying processes. As SO_2 oxidation was indicated through the detection of sulphates (e.g., gypsum crystals of typical acicular habit) on the sample surfaces, and as SO_2 oxidation is associated with acidification of the environment, it is also possible that the fissures formed as a result of denaturalization of the binders. The FTIR analysis confirmed the presence of chemical deterioration, at least in the samples containing egg yolk.

In the CIN-C-R, the colour changes were determined by salt precipitation and degradation in the binder (i.e., formation of fissures in both binders), although darkening was also observed in isolated areas. Different possible pathways for blackening have been proposed [39–45]. In the present study, it is possible that the chloride (15.8 mg/L Cl^{-}) present

in the water of the climatic chamber and detected in all the aged paints (HE and CIN), was involved in darkening of some of the CIN-based paints. Regarding the colorimetric changes in the CIN-based paints, the ΔE^*_{ab} was higher in those containing egg yolk than in those containing rabbit glue. However, the change in colour was not related to the pigment particle size, as ΔE^*_{ab} was highest in the CIN-C paints and lowest in the CIN-M paints.

In the HE-based paints, the most intense colorimetric change was detected in the rabbit glue-based paint, due to the deposition of abundant white salts on the surface (visible to the naked eye). Importantly, in addition to the colorimetric changes, precipitation of salts on the sample surfaces also contributed to changes in reflectance. In general, reflectance was higher in the aged paints, as observed in previous studies involving tempera paints mock-ups made of azurite, malachite, lapis lazuli and smalt [27,28].

The roughness was not related to either the binder or particle size as, owing to the large standard deviations, only the difference of the Rz value between the CIN-M-E paint before and after the test was statistically significant. The variation in roughness can probably be attributed to the salt deposition and formation of fissures, as previously observed [27,28].

A notable fact is that differences in behaviour have been found between paints made with hematite and those with cinnabar; but also, within each group, opposite results were found depending on whether the binder was egg yolk or rabbit glue. This fact indicates that the pigment-binder tandem is a variable that could influence the susceptibility to deterioration, at least regarding the response of exposure to SO_2. These findings are consistent with those of previous studies [27,28] showing that the pigment-binder interaction influences the reflectance of tempera paints aged by exposure to SO_2, due to the neoformation of minerals and the changes in the pigments and/or binder.

4. Conclusions

Red tempera paint mock-ups containing hematite or cinnabar (the latter of different particle sizes) mixed with either egg yolk or rabbit glue as binder were exposed to a SO_2-rich atmosphere for two months (25 °C; 45% RH). Physical changes in appearance, colour, gloss, reflectance, roughness and micro-texture were evaluated in all aged paint samples. Likewise, the composition of the paint mock-ups was analysed before and after the SO_2 aging test by means of XRPD (mineralogical), ATR-FTIR (molecular) and SEM-EDS (elemental) analysis. In addition, the binders and the pigments were also individually characterized by XRPD and SEM-EDS analysis.

After SO_2 exposition, darkening was detected in the hematite tempera mock-ups and in the CIN-C tempera mock-up, although in any case, the formation of new mineral phases, responsible for this colour change, were detected. SEM allowed to confirm the formation of sulphate-rich deposits on the surfaces of all the exposed mock-ups, with gypsum the most probable phase, taking into account the elemental composition and the habit of the crystals, although the formation of other sulphated salts is not ruled out. Salt deposits were particularly abundant on the cinnabar-based paints containing egg yolk, as well as on the hematite-based paints containing rabbit glue. SEM analyses confirmed the formation of fissures in all the samples after SO_2 exposition.

The physical changes detected in the paints, specifically in the colour and reflectance, are attributed to the precipitation of salt deposits and to the formation of fissures. Differences in gloss were minimal, and differences in roughness were not statically significant. For the cinnabar-based paints, the colorimetric changes were greatest in the paints containing egg yolk, while the total colour difference was greatest in the hematite-based paints containing rabbit glue, coinciding with the samples with the largest amounts of salts deposited on the surface. An influence of the grain size of the pigment on the susceptibility to deterioration of cinnabar tempera to SO_2 exposure has not been detected, since no relationship between the intensity of the colorimetric changes and roughness, or between the amount of saline deposits and the grain size was found.

The formation of sulphate salts in the mock-ups exposed to SO_2 confirmed that hematite and cinnabar-based tempera paints are reactive to SO_2 gas. The sulphur that

makes up the sulphated deposits comes from the SO_2 exposure gas, since no mineralogical changes have been found in the cinnabar raw pigment. Regarding Ca and other alkaline and alkaline earth elements that are present in sulphate deposits formed after SO_2 exposure, different sources are suggested: either from the binders themselves or from the impurities present in the pigments. However, contamination from the water used in the chamber is not ruled out.

It should be noted that the atmospheric concentrations of SO_2 have decreased substantially worldwide in the last few decades. However, many painted artworks have already been subjected to prolonged exposure to this air pollutant, and information about the adverse effects on such paintings will be useful in decision-making regarding preventive conservation measures.

Supplementary Materials: The following supporting information can be downloaded at: https://www.mdpi.com/article/10.3390/min13020289/s1, Figure S1: Diffractograms of hematite paint-mock-ups before and after SO_2-exposure test. Figure S2: Diffractograms of CIN-ST paint-mock-ups before and after SO_2-exposure test. Figure S3: Diffractograms of CIN-EF paint-mock-ups before and after SO_2-exposure test. Figure S4: Diffractograms of CIN-M paint-mock-ups before and after SO_2-exposure test. Figure S5: Diffractograms of CIN-C paint-mock-ups before and after SO_2-exposure test.

Author Contributions: Conceptualization, J.S.P.-A., T.R. and C.C.; methodology, J.S.P.-A., D.J.-D., A.D., L.D.V. and A.M.; software, J.S.P.-A., T.R., C.C., L.D.V. and A.M.; validation, J.S.P.-A., T.R. and C.C.; formal analysis, J.S.P.-A., L.D.V. and A.M.; investigation, J.S.P.-A., T.R., C.C. and A.D.; resources, J.S.P.-A., T.R., C.C. and A.D.; data curation, J.S.P.-A., D.J.-D., L.D.V. and A.M.; writing—original draft preparation, J.S.P.-A. and D.J.-D.; writing—review and editing, T.R., C.C. and A.D.; visualization, J.S.P.-A., T.R. and C.C.; supervision, J.S.P.-A.; project administration, J.S.P.-A., T.R. and C.C.; funding acquisition, J.S.P.-A., T.R. and C.C. All authors have read and agreed to the published version of the manuscript.

Funding: This research was funded by the Galician Research Project LASERING-PH (ED431F 2022/07), the Spanish Research Projects LASERING-PH (PID2021-123395OA-I00), AERIMPACT (CGL2012-30729) and EXPOAIR (P12-FQM-1889), the European Regional Development Fund (ERDF) and the Andalusian Research Group RNM-179. J.S.P.-A. and D.J.-D. were supported by the Ministry of Science and Innovation, Government of Spain through the project RYC2020-028902-I.

Data Availability Statement: Not applicable.

Acknowledgments: The authors thank Alberto Ramil for helpful assistance in acquiring hyperspectral images. Funding was provided by open access charge: Universidade de Vigo/CISUG. They also acknowledge the support of the CERENA (strategic project FCTUID/ECI/04028/2019). Analyses were performed in the CACTI (Centro de Apoyo a la Investigación) Research Support Centre at the University of Vigo. The accelerated SO_2 aging tests were performed in the Instituto Superior Tecnico (Lisbon, Portugal).

Conflicts of Interest: The authors declare no conflict of interest.

References

1. Maguregui, M.; Knuutinen, U.; Martínez-Arkarazo, I.; Castro, K.; Madariaga, J.M. Thermodynamic and spectroscopic speciation to explain the blackening process of hematite formed by atmospheric SO_2 impact: The case of Marcus Lucretius House (Pompeii). *Anal. Chem.* **2011**, *83*, 3319–3326. [CrossRef]
2. Maguregui, M.; Castro, K.; Morillas, H.; Trebolazabala, J.; Knuutinen, U.; Wiesinger, R.; Schreiner, M.; Madariaga, J.M. Multi-analytical approach to explain the darkening process of hematite pigment in paintings from ancient Pompeii after accelerated weathering experiments. *Anal. Methods* **2014**, *6*, 372. [CrossRef]
3. Herrera, A.; Navas, N.; Cardell, C. An evaluation of the impact of urban air pollution on paint dosimeters by tracking changes in the lipid MALDI-TOF mass spectra profile. *Talanta* **2016**, *155*, 53–61. [CrossRef] [PubMed]
4. Douglas-Jones, R.; Hughes, J.J.; Jones, S.; Yarrow, T. Science, value and material decay in the conservation of historic environments. *J. Cult. Herit.* **2016**, *21*, 823–833. [CrossRef]
5. Rivas, T.; Pozo-Antonio, J.S.; Barral, D.; Martínez, J.; Cardell, C. Statistical analysis of colour changes in tempera paints mock-ups exposed to urban and marine environment. *Meas. J. Int. Meas. Confed.* **2018**, *118*, 298–310. [CrossRef]

6. Pérez-Diez, S.; Pitarch-Martí, A.; Giakoumaki, A.; Prieto-Taboada, N.; Fdez-Ortiz de Vallejuelo, S.; Martellone, A.; De Nidris, B.; Osanna, M.; Madariaga, J.M.; Maguregui, M. When red turns black: Influence of the 79 AD volcanic eruption and burial environment on the blackening/darkening of Pompeian cinnabar. *Anal. Chem.* **2021**, *93*, 15870–15877. [CrossRef]
7. Williams, E.L.; Grosjean, E.; Grosjean, D. Exposure of Artists´Colorants to Sulfur Dioxide. *J. Am. Inst. Conserv.* **2013**, *32*, 291–310. [CrossRef]
8. Grosjean, D.; Whitmore, P.M.; de Moor, C.P.; Cass, R.; Druzik, J.R. Fading of Alizarin and related artists' pigments by atmospheric ozone: Reaction products and mechanism. *Environ. Sci. Technol.* **1987**, *21*, 635–643. [CrossRef]
9. Grosjean, D.; Whitmore, P.M.; Cass, R.; Druzik, J.R. Ozone fading of natural organic colorants: Mechanisms and products of the reaction of ozone with Indigos. *Environ. Sci. Technol.* **1988**, *22*, 292–298. [CrossRef]
10. Grosjean, D.; Whitmore, P.M.; De Moor, C.P.; Cass, R.; Druzik, J.R. Ozone fading of natural organic colorants: Mechanisms and products of the reaction of ozone with Curcumin. *Environ. Sci. Technol.* **1988**, *22*, 1357–1361. [CrossRef]
11. Grosjean, D.; Grosjean, E.; Williams, E.L., II. Fading of artists´colorants by a mixture of photochemical oxidant. *Atmos. Environ.* **1993**, *27A*, 765–772. [CrossRef]
12. Whitmore, P.M.; Cass, G.R. The ozone fading of traditional Japanese colorants. *Stud. Conserv.* **1988**, *33*, 29–40.
13. Whitmore, P.M.; Cass, G.R. The fading of artists colorants by exposure to atmospheric nitrogen dioxide. *Stud. Conserv.* **1989**, *34*, 85–97.
14. Odlyha, M.; Cohen, N.S.; Foster, G.M.; West, R.H. Dosimetry of paintings: Determination of the degree of chemical change in museum exposed test paintings (azurite tempera) by thermal and spectroscopic analysis. *Thermochim. Acta* **2000**, *365*, 53–63. [CrossRef]
15. Odlyha, M.; Cohen, N.S.; Foster, G.M. Dosimetry of paintings: Determination of the degree of chemical change in museum exposed test paintings (smalt tempera) by thermal analysis. *Thermochim. Acta* **2000**, *365*, 35–44. [CrossRef]
16. Van den Brink, O.F.; Eijkel, G.B.; Boon, J.J. Dosimetry of paintings: Determination of the degree of chemical change in museum-exposed test paintings by mass spectroscopy. *Thermochim. Acta* **2000**, *365*, 1–23. [CrossRef]
17. Bacci, M.; Picollo, M.; Porcinai, S.; Radicati, B. Evaluation of the museum environmental risk by means of tempera-painted dosimeters. *Thermochim. Acta* **2000**, *365*, 25–34. [CrossRef]
18. Arbizzani, R.; Casellato, U.; Fiorin, E.; Nodari, L.; Russo, U.; Vigato, P.A. Decay markers for the preventative conservation and maintenance of paintings. *J. Cult. Herit.* **2004**, *5*, 167–182. [CrossRef]
19. West, R.H.; Odlyha, M.; Pratt, K.; Roberts, A.; Hutton, S. Monitoring the environmental degradation of paint dosimeters used to assess risk for fine art paintings on display by XPS. *Surf. Interface Anal.* **2004**, *36*, 862–865. [CrossRef]
20. Edwards, R.D.; Lam, N.L.; Zhang, L.; Johnson, M.A.; Kleinman, M.T. Nitrogen dioxide and ozone as factors in the availability of lied from lead-based paints. *Environ. Sci. Technol.* **2009**, *43*, 8516–8521. [CrossRef]
21. EEA, European Environment Agency. *Air Pollution Fact Sheet 2013—Spain*; European Environment Agency: Copenhagen, Denmark, 2013.
22. Urosevic, M.; Yebra-Rodríguez, A.; Sebastián-Pardo, E.; Cardell, C. Black soiling of an architectural limestone during two-year term exposure to urban air in the city of granada (S spain). *Sci. Total Environ.* **2012**, *414*, 564–575. [CrossRef] [PubMed]
23. Rivas, T.; Pozo, S.; Paz, M. Sulfur and oxygen isotope analysis to identify sources of sulfur in gypsum-rich black crusts developed on granites. *Sci. Total Environ.* **2014**, *482–483*, 137–147. [CrossRef] [PubMed]
24. Pozo-Antonio, J.S.; Pereira, M.F.C.; Rocha, C.S.A. Microscopic characterisation of black crusts on different substrates. *Sci. Total Environ.* **2017**, *584–585*, 291–306. [CrossRef] [PubMed]
25. Pozo-Antonio, J.S.; Barral, D.; Herrera, A.; Elert, K.; Rivas, T.; Cardell, C. Effect of tempera paint composition on their superficial physical properties—Application of interferometric profilometry and hyperspectral imaging techniques. *Prog. Org. Coat.* **2018**, *117C*, 56–68. [CrossRef]
26. Pérez, M.; Castro, K.; Rodríguez, M.; Olazabal, M.; Madariaga, J. A critical analysis of commercial pigments. In Proceedings of the ART 2002, 7th International Conference on Non-Destructive Testing and Microanalysis for the Diagnostics and Conservation of the Cultural and Environmental Heritage, Antwerp, Belgium, 2–6 June 2002; pp. 173–182.
27. Pozo-Antonio, J.S.; Rivas, T.; Dionisio, A.; Barral, D.; Cardell, C. Effect of a SO_2 rich atmosphere on tempera paint mock-ups. Part 1: Accelerated aging of smalt and lapis lazuli-based paints. *Minerals* **2020**, *10*, 427. [CrossRef]
28. Pozo-Antonio, J.S.; Cardell, C.; Dionisio, A.; Barral, D.; Rivas, T. Effect of a SO_2 Rich Atmosphere on Tempera Paint Mock-Ups. Part 2: Accelerated Aging of Azurite- and Malachite-Based Paints. *Minerals* **2020**, *10*, 424. [CrossRef]
29. Cardell, C.; Herrera, A.; Guerra, I.; Navas, N.; Simón, L.R.; Elert, K. Pigment-size effect on the physicochemical behavior of azurite-tempera dosimeters upon natural and accelerated photo aging. *Dyes Pigment.* **2017**, *141*, 53–65. [CrossRef]
30. Han, K.; Nam, J.Y.; Ji, J.E.; Kang, D.; Lee, H.; Baek, N. Existence of nanoparticles in azurite and malachite pigments by Raman spectroscopy and X-ray diffraction studies. *Dyes Pigment.* **2016**, *133*, 232–237. [CrossRef]
31. Herrera, A.; Cardell, C.; Pozo-Antonio, J.S.; Burgos-Cara, A.; Elert, K. Effect of proteinaceous binder on pollution-induced sulfation of lime-based tempera paints. *Prog. Org. Coat.* **2018**, *123*, 99–110. [CrossRef]
32. Pomies, M.P.; Menu, M.; Vignaud, C. Red palaeolithic pigmnets: Natural hematite or heated goethite? *Archaeeometry* **1999**, *41*, 275–285. [CrossRef]
33. Giustetto, R.; Dario, G.; Diana, E. Decay of red pigments on a wall painting adorning the church of 'San Francesco Dei Capuccini'in Racconigi (Italy). *Archaeom. Surv. Restor. Interv.* **2018**, *18*, 65–80.

34. Cristini, O.; Kinowski, C.; Turrell, S. A detailed micro-Raman spectroscopic study of wall paintings of the period AD 100–200: Effect of atmospheric conditions on the alteration of samples. *J. Raman Spectrosc.* **2010**, *41*, 1410–1417. [CrossRef]
35. Coccato, A.; Moens, L.; Vandenabeele, P. On the stability of mediaeval inorganic pigments: A literature review of the effect of climate, material selection, biological activity, analysis and conservation treatments. *Herit. Sci.* **2017**, *5*, 1–25. [CrossRef]
36. Pailhé, N.; Wattiaux, A.; Gaudon, M.; Demourgues, A. Impact of structural features on pigment properties of α-Fe2O3 haematite. *J. Solid State Chem.* **2008**, *181*, 2697–2704. [CrossRef]
37. Hirst, K. Cinnabar-The Ancient Pigment of Mercury. Available online: https://www.thoughtco.com/cinnabar-the-ancient-pigment-of-mercury-170556 (accessed on 9 September 2022).
38. Gettens, R.J.; Feller, R.L.; Chase, W.T. Vermilion and cinnabar. *Stud. Conserv.* **1972**, *17*, 45–69.
39. Vandenabeele, P.; Lambert, K.; Matthys, S.; Schudel, W.; Bergmans, A.; Moens, L. In situ analysis of mediaeval wall paintings: A challenge for mobile. Raman spectroscopy. *Anal. Bioanal. Chem.* **2005**, *383*, 707–712. [CrossRef] [PubMed]
40. Yu, J.; Warren, W.S.; Fischer, M.C. Visualization of vermilion degradation using pump-probe microscopy. *Sci. Adv.* **2019**, *5*, eaaw3136. [CrossRef]
41. Dreyer, R.M. Darkening of cinnabar in sunlight. *Am. Mineral.* **1938**, *23*, 457–460.
42. Anaf, W.; Janssens, K.; De Wael, K. Formation of metallic mercury during photodegradation/photodarkening of α-HgS: Electrochemical evidence. *Angew. Chem. Int. Ed.* **2013**, *125*, 12800–12803. [CrossRef]
43. Da Pieve, F.; Hogan, C.; Lamoen, D.; Verbeeck, J.; Vanmeert, F.; Radepont, M.; Cotte, M.; Janssens, K.; Gonze, X.; Van Tendeloo, G. Casting light on the darkening of colors in historical paintings. *Phys. Rev. Lett.* **2013**, *111*, 208302. [CrossRef]
44. Kegelman Neiman, M.; Balonis, M.; Kakoulli, I. Cinnabar alteration in archaeological wall paintings: An experimental and theoretical approach. *Appl. Phys.* **2015**, *121*, 915–938. [CrossRef]
45. Elert, K.; Pérez Mendoza, M.; Cardell, C. Direct evidence for metallic mercury causing photo-induced darkening of red cinnabar tempera paints. *Commun. Chem.* **2021**, *4*, 1–10. [CrossRef] [PubMed]
46. Dickson, F.W.; Tunell, G. The stability relations of cinnabar and metacinnabar. *Am. Mineral.* **1959**, *44*, 471–487.
47. Nusimovici, M.A.; Meskaoui, A. Raman scattering by α-HgS (cinnabar). *Phys. Stat. Sol. B* **1973**, *58*, 121–125. [CrossRef]
48. Pal, B.; Ikeda, S.; Ohtani, B. Photoinduced chemical reactions on natural single crystals and synthesized crystallites of mercury (II) sulfide in aqueous solution containing naturally occurring amino acids. *Inorg. Chem.* **2003**, *42*, 1518–1524. [CrossRef] [PubMed]
49. Ballirano, P.; Botticelli, M.; Maras, A. Thermal behaviour of cinnabar, α-HgS, and the kinetics of the β-HgS (metacinnabar) → α-HgS conversion at room temperature. *Eur. J. Mineral.* **2013**, *25*, 957–965. [CrossRef]
50. Miguel, C.; Pinto, J.V.; Clarke, M.; Melo, M.J. The alchemy of red mercury sulphide: The production of vermilion for medieval art. *Dyes Pigm.* **2014**, *102*, 210–217. [CrossRef]
51. Pacheco, F. *El Arte de la Pintura*; Cátedra: Madrid, Spain, 1990.
52. *CIE Publication 15-2*; Colorimetry. CIE Central Bureau: Vienna, Austria, 1986.
53. *CIE S014-4/E*; Colorimetry Part 4: CIE 1976 L*a*b* Colour Space. Commission Internationale de l'eclairage. CIE Central Bureau: Vienna, Austria, 2007.
54. *UNE-EN ISO 4288*; Geometrical Product Specifications (GPS). In Surface Texture: Profile Method, Terms, Definitions and Surface Texture Parameters. Asociación Española de Normalización y Certificación. AENOR: Madrid, España, 1999.
55. *BS EN 828-Adhesives*; Wettability. In Determination by Measurement of Contact Angle and Surface Free Energy of Solid Surface. European Committee for Standardization. CEN: Brussels, Belgium, 2013.
56. Mokrzycki, W.; Tatol, M. Color difference DeltaE—A survey. *Mach. Graph. Vis.* **2011**, *20*, 383–411.
57. Fuertes, S.; Laca, A.; Oulego, P.; Paredes, B.; Rendueles, M.; Díaz, M. Development and characterization of egg yolk and egg yolk fractions edible films. *Food Hydrocoll.* **2017**, *70*, 229–239. [CrossRef]
58. Mazzeo, R.; Prati, S.; Quaranta, M.; Joseph, E.; Kendix, E.; Galeotti, M. Attenuated total reflection microFTIR characterization of pigment-binder interaction in reconstructed paint flims. *Anal. Bioanal. Chem.* **2008**, *392*, 65–76. [CrossRef]
59. Nodari, L.; Ricciardi, P. Non-invasive identification of paint binders in illuminated manuscripts by ERFTIR spectroscopy: A systematic study of the influence of different pigments on the binders' characteristic spectral features. *Herit. Sci.* **2019**, *7*, 7. [CrossRef]
60. Wang, Q.; Sanad, W.; Miller, L.M.; Voigt, A.; Klingel, K.; Kandolf, R.; Stangl, K.; Baumann, G. Infrared imaging of compositional changes in inflammatory cardiomyopathy. *Vib. Spectrosc.* **2005**, *38*, 217–222. [CrossRef]
61. Pellegrini, D.; Duce, C.; Bonaduce, I.; Biagi, S.; Ghezzi, L.; Colombini, M.P.; Tinè, M.R.; Bramanti, E. Fourier transform infrared spectroscopic study of rabbit glue/inorganic pigments mixtures in fresh and aged reference paint reconstructions. *Microchem. J.* **2016**, *124*, 31–35. [CrossRef]
62. Nasrazadani, S.; Namduri, H. Study of phase transformation in iron oxides using laser induced breakdown spectroscpy. *Spectrochim. Acta—Part B At. Spectrosc.* **2006**, *61*, 565–571. [CrossRef]
63. Ji, J.; Ge, Y.; Balsam, W.; Damuth, J.E.; Chen, J. Rapid identification of dolomite using a fourier transform infrared spectrophotometer (FTIR): A fast method for identifying heinrich events in IODP site U1308. *Mar. Geol.* **2009**, *258*, 60–68. [CrossRef]
64. Vila, A.; Garcia, J.F. Analysis of the Chemical Composition of Red Pigments and Inks for the Characterization and Differentiation of Contemporary Prints. *Anal. Lett.* **2012**, *45*, 1274. [CrossRef]
65. Socrates, G. *Infrared and Raman Characteristic Group Frequencies: Tables and Charts*, 3rd ed.; Wiley: Hoboken, NJ, USA, 2004; 368p, ISBN 978-0-470-09307-8.

66. Papuc, C.; Goran, G.V.; Predescu, C.N.; Nicorescu, V. Mechanisms of oxidative processes in meat and toxicity induced by postprandial degradation products: A review. *Compr. Rev. Food Sci. Food Saf.* **2017**, *16*, 96–123. [CrossRef]
67. Bico, J.; Thiele, U.; Quere, D. Wetting of textured surfaces, Colloids Surf. A Physicochem. *Eng. Asp.* **2002**, *206*, 41–46. [CrossRef]
68. Giusetto, R.; Pastero, L.; Aquilano, D. Potential effects of the shape of gypsum aggregates on the early sulfation of marble and travertine. *J. Build. Eng.* **2020**, *32*, 101794. [CrossRef]
69. Cotte, M.; Susini, J.; Metrich, N.; Moscato, A.; Gratziu, C.; Bertagnini, A.; Pagano, M. Blackening of pompeian cinnabar paintings: X-ray microspectroscopy analysis. *Anal. Chem.* **2006**, *78*, 7484–7492. [CrossRef]
70. Mohamed, A.-M.O.; Paleologos, E.K. Chapter 4—The Soil System. In *Paleologos, Fundamentals of Geoenvironmental Engineering, Butterworth-Heinemann*; Mohamed, A.-M.O., Evan, K., Eds.; Butterworth-Heinemann: Oxford, UK, 2018; pp. 89–127. ISBN 9780128048306. [CrossRef]